L. Barbé
B. Bayle
M. de Mathelin
LSIIT, UMR CNRS 7005, University of Strasbourg, France
{baube, bernard, demath}@eavr.u-strasbg.fr

A. Gangi
Radiology Dept. B, University Hospitals of Strasbourg, France
gangi@rad6.u-strasbg.fr

In Vivo Model Estimation and Haptic Characterization of Needle Insertions

Abstract

During percutaneous interventions, the haptic perception of transitions and ruptures in the tissues is fundamental. In the medical robotics context, these events should be conveyed to a remote telemanipulating practitioner or should be taken into account in a robotic control scheme. However, this problem is extremely complex given the nature and the variety of tissues involved in percutaneous procedures. In this article, in vivo percutaneous experiments associated with an online model estimation of the interaction between tissues and a surgical needle are presented for the first time. The estimation scheme is then used to provide a robust method to automatically detect the transitions that occur during needle insertion. Finally, the principle of a modified teleoperation scheme that would allow better haptic discrimination of ruptures is proposed and illustrated.

KEY WORDS—Medical robots, systems, telerobotics

1. Introduction

1.1. Motivation

Interventional radiology is a fast developing medical field in which specialists use per-operative medical imaging techniques (CT-scan, C-arm, Ultrasound, MRI, . . .) to guide the insertion of surgical needles into target internal organs. It allows minimally invasive local treatments (Rhim et al. 2001). Unfortunately, these procedures have two important drawbacks. First, it is difficult to precisely place the needle tip into the target tissue. Second, during a CT-scan or a C-arm guided operation, the radiologist is exposed to X-ray radiations. Therefore, robotized needle insertion systems have recently appeared (Stoianovici et al. 1997; Kronreif et al. 2003; Hong et al. 2004; Maurin et al. 2004a) in order to simultaneously increase the precision of needle positioning and to protect the physician from harmful radiations.

In this context, an understanding of the interactions between surgical needles and living tissues has become a challenging task. Indeed, soft tissue dynamic properties are important to design the robot control strategy, particularly in the case of force control or force feedback teleoperation. Online estimated environment properties can be taken into account to improve force feedback quality (Diolaiti 2005; De Gersem 2005). In the case of percutaneous interventions, the identification of characteristic properties in the force signal, in particular the detection of abrupt changes, could be rendered by an adequate modality (possibly sound, image or amplified haptic feedback).

Nevertheless, the characterization of these interactions remains a complex task, for different reasons. First, the different layers crossed by the needle (skin, fat, muscles, organs) are inhomogeneous and so the mechanical properties of each layer cannot be described by constant parameters. Second, these parameters values may be patient dependent and are linked to a particular needle type. Also, when the needle is inserted in a body, the elementary contributions of the different tissues are superimposed. Finally, since the needle pierces the tissues, the interaction is clearly nonlinear. An illustrative example is obtained when the needle perforates an organ wall, which provokes an almost instantaneous variation in the exerted force profile. For all these reasons, haptic modeling, which states the relations between motions and interaction forces, is a difficult task in the case of needle insertions.

1.2. Needle insertion description

In order to characterize the interaction between a needle and soft living tissues, we first describe a puncture into a single

The International Journal of Robotics Research
Vol. 26, No. 11–12, November/December 2007, pp. 1283–1301
DOI: 10.1177/0278364907082666

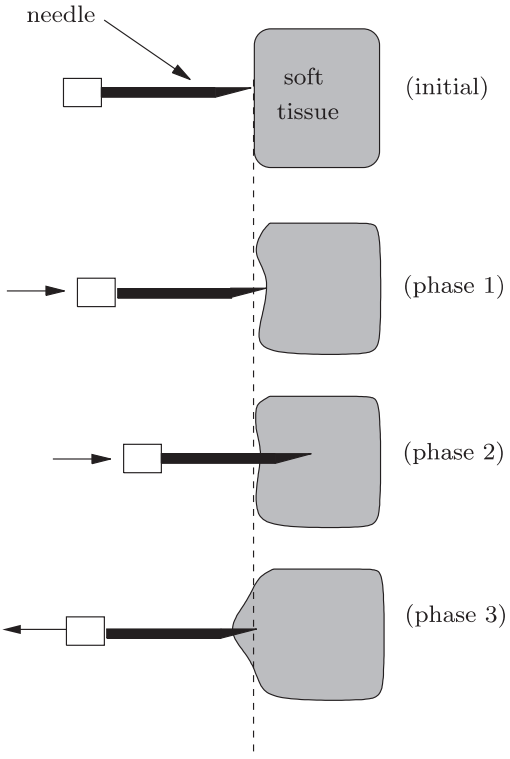

Fig. 1. Needle insertion into a single layer soft tissue.

layer sample. Assuming that the needle tip is initially motionless and in contact with the surface of the tissue, then, the needle insertion is a three phase procedure (Simone and Okamura 2002), as illustrated in Figure 1:

- phase 1: the needle pushes the tissue surface which becomes deformed;
- phase 2: when the applied force reaches a given energetic threshold (Heverly et al. 2005), the needle penetrates into the tissue by cutting its surface. While the needle is inserted, the friction forces attract the skin along the needle shaft;
- phase 3: the needle is extracted from the tissue. Again, the tissue is attracted in the needle motion direction. Consequently, the position of the needle when it is completely extracted does not correspond to the initial contact position.

Phase 1 corresponds to a viscoelastic interaction, as described by Okamura et al. (2004). Then, the interaction forces during the insertion phase are due to the combined effects of cutting, friction, and to the relaxation of the skin after the puncture. Finally, during needle extraction, the interaction between the needle and the tissue is only due to friction.

1.3. Related Work

The use of force signal characteristics in the medical field has already been demonstrated. Zivanovic and Davies (2000) use the needle insertion force profile to localize veins and to detect vein wall breakthrough. They apply this detection to a prototype blood sampling machine. Brett et al. (2000) mimic the manual epidural procedure by using pressure transitions as clues to detect the insertion of a needle in the epidural space. Realistic force profiles are also necessary to design needle or catheter insertion simulators. DiMaio and Salcudean (2003) give a very good overview of existing work. In the teleoperation field, De Gersem et al. (2005) prove that an interaction model estimation can notably enhance stiffness perception in force feedback procedures.

Concerning haptic modeling of needle insertion, pioneer work recently appeared, principally in the medical robotics field, both for the purpose of simulation and teleoperation of a robotic needle holder. From a classical biomechanics point of view, homogeneous materials can be studied by rheological methods. Different kinds of stimuli are applied to samples of material and the corresponding effects are measured. Kobayashi et al. (2004) characterize the dynamical and nonlinear properties of the liver from viscoelastic and creep tests. To do this, the authors use a rheometer to strain hog liver samples. Although, the extrapolation of such results to a whole organ may be controversial, one can expect to obtain a good approximation in the case of the liver since it is considered as one of the most homogeneous organs. The effects of tissue cutting have also to be considered. Okamura et al. (2004) study the forces involved in the needle penetration and withdrawal phases. The insertion into bovine liver samples is controlled by a robotic translator and the associated forces and displacements are measured. Using a detailed modeling of the force components, the authors describe a methodology to separate the contributions of stiffness, friction and cutting forces, in order to derive a complete force model. The results obtained are convincing, but as pointed out by the authors, the proposed methodology involves different specific *ex vivo* tests to adjust parameters to patient variability.

In the following, we will assume for obvious reasons that insertion of the needle in a patient should be strictly limited to the necessary medical task. From this point of view, given the inter- patient variability, the online identification of a needle insertion model from data collected during the medical act itself is required. In order to separate the different components of needle insertion forces, Washio and Chinzei (2004) present a dedicated force sensor built from two coaxial load cells. One measures the friction on a sheath covering the needle and the other measures the remaining efforts on the blade, i.e. the cutting and damping forces. DiMaio and Salcudean (2003) estimate an elastostatic linear model derived from the needle tip force and position measurements and from the deformation of the pierced material. Deformations are given by markers

placed on the surface of the material. Again, it is difficult to use this procedure in clinical conditions, specially in the case of internal organs.

Two recent contributions to the online estimation of interactions with soft materials have been reported. In the context of the interaction of a robot with a soft environment, Diolaiti et al. (2005) focus on the online estimation of viscoelastic linear and nonlinear models. The proposed methodology is of interest, although results are given for small motions of a translator system in contact with thin layers of stiff and soft artificial samples. In the medical field, De Gersem (2005) uses an extended Kalman filter to estimate online the stiffness of the interaction of laparoscopic tools in teleoperated palpation with force feedback. Though these methods were applied to viscoelastic interactions, i.e. without cutting, they are quite interesting and inspired the present work.

1.4. Objectives and Outline

In this article, a model of needle insertion is identified online and used for the detection of nonlinearities in the force signal during percutaneous procedures. The study is based on the online reconstruction of the force exerted by the needle. Since *in vivo* conditions are critical to derive realistic models (Ottensmeyer and Salisbury 2001), experiments are done for the first time in operation conditions. These experiments highlight the quality and applicability of the model estimation compared to classical filtering and thresholding. The paper also shows how this haptic characterization could be used in a force feedback teleoperation scheme.

The paper is organized as follows. In section 2, standard linear and nonlinear models are presented and the specificities of needle insertions are discussed. The robust algorithms used to estimate a varying parameters model are introduced. Section 3 details *in vivo* experiments and presents characteristic results. Section 4 discusses the detection of nonlinearities in the force signal. Section 5 describes a way to use this haptic characterization of needle insertions. It consists in the simulation of a haptically augmented force feedback teleoperation scheme. Finally, the major contributions of this work are summarized in the conclusion and future research directions are proposed.

2. Modeling and Estimation

Given the authors'interest in the treatment of liver cancers in interventional radiology, this study is focused on this organ. However, the proposed methods apply to a large range of organs.

2.1. Modeling of Needle Interactions

The simple case of the insertion of a needle into a one layer soft tissue is considered. As previously underlined, the behavior of the tissue during the first phase of the insertion (see Figure 1) can be approximated by a viscoelastic model. According to Fung (1993), most living tissues have viscoelastic behavior as long as small motions are considered. In the case of uniaxial displacements, a viscoelastic model relates the interaction force and the displacement between two bodies. Linear soft tissue viscoelastic models are often described by serial or parallel combinations of springs and dashpots (Maurel 1998). The classical models built from an equivalent spring and an equivalent viscous element are the serial Maxwell model and the parallel Kelvin–Voigt (KV) model. This latter is certainly the most commonly used. For use in the needle insertion context, the KV model can be written as:

$$f = \begin{cases} -(Kp + Bv), & \text{if } p > 0 \\ 0, & \text{if } p \leq 0 \end{cases} \tag{1}$$

where f is the force exerted on the tissue, p and v represent its position and velocity, respectively, K is the stiffness coefficient and B the damping coefficient. The position $p = 0$ corresponds to the initial contact point. However, the representation of organic tissues by a linear model is generally not adequate and the force usually varies in a nonlinear way regardless of the tissue motion. The Hunt–Crossley (HC) model (Hunt and Crossley 1975) intrinsically takes into account the penetration depth between two bodies. It can be written as:

$$f = \begin{cases} -(\mu p^n + \lambda p^n v), & \text{if } p > 0 \\ 0, & \text{if } p \leq 0 \end{cases} \tag{2}$$

where μ, λ and n are constant parameters that depend on the material properties. Then, during the viscoelastic phase of the insertion, the measured force can be expressed by either the KV or the HC model, although the latter is probably the most suitable, as tissue deformation is often important. In this case, the force profile is polynomial, as mentioned in (Okamura et al. 2004) and (Maurin et al. 2004b).

After puncture, it is more difficult to express f than in the simple viscoelastic case. Okamura et al. (2004) assume that the measured force is composed of a friction force and a cutting force after the liver capsule puncture. In fact, the cutting force that is dominant in the results presented is a combination of the actual cutting force and of the stiffness force resulting from the persisting tissue compression. Indeed, whereas friction is identified by periodic stimuli of liver samples, it remains difficult to separate the contribution of cutting and pressing.

As we aim at making this identification without markers on the skin, the precise identification of such a physically inspired model is definitively out of reach. A first solution would consist in grouping some of the terms of the model as proposed by Okamura et al. Another possibility is to use a simpler but less accurate model. Yen et al. (1996) propose a model of tissue for needle insertion based on a KV model with piecewise constant parameters. Since the needle punctures several inhomogeneous layers, which all have different behaviors, this appears

quite sensible. However, the difficulty is to detect the organ transitions instants or finer details like, for instance, small vessel ruptures. Consequently, we decided to use a model in the form of the KV model, but for which the parameters K and B are time-varying and depend on the position and the velocity of the needle tip, i.e. such that:

$$f = \begin{cases} -(K(p,\ v,\ t)p + B(p,\ v,\ t)v), & \text{if } p > 0 \\ 0, & \text{if } p \leq 0 \end{cases} \tag{3}$$

In the following we term this model the KV Generalized (KVG) model.

It is necessary to make the following comments. First, the proposed KVG model cannot be considered as physically accurate, since it does not explicitly take into account tissue deformations, friction or cutting. It means that the K and B parameters are no longer rigorously stiffness and viscous friction coefficients. However, as will be explained in the following, the KVG model allows one to reconstruct the force precisely with a simple parametric description, which is sufficient for the robust detection of force transitions. Second, even if the HC nonlinear model was used, it could not be described by constant parameters μ, λ and n during the whole needle insertion procedure. Note that the KVG model (3) includes the HC model (2) if K and B are defined as:

$$\begin{cases} K(p,\ v,\ t) &= \mu(p,\ v,\ t)p^{n-1} \\ B(p,\ v,\ t) &= \lambda(p,\ v,\ t)p^{n} \end{cases} \tag{4}$$

Therefore, hereafter the KVG model will be used.

2.2. Robust Parameters Estimation

To estimate the mechanical parameters of a biomechanical model, different methods can be considered. When physical modeling is possible, the parameters are generally derived from typical biomechanical values. In the case of percutaneous needle insertions, this method does not work since a large variety of patients need to be precisely characterized. On the contrary, the online estimation of a simple model is not as physically relevant but it allows real-time information on the force evolution. In the following, we focus on recursive estimation techniques for percutaneous procedures, as originally proposed in (Barbé et al. 2006).

2.2.1. Problem Formulation

Recursive parametric estimation algorithms (Goodwin and Sin 1984) are usually based on a discrete time linear parameterization of the system:

$$y_{k+1} = \varphi_k^T \theta_k^* + w_{k+1} \tag{5}$$

where θ_k^* is the vector of unknown parameters to be estimated at time k, y_k is the measured output signal, φ_k is the regression vector build from measured signals (previous outputs, exogenous inputs). The output measurement noise is represented by the signal w_k with zero mean value.

Using the estimation $\hat{\theta}_k$ of θ_k^*, at time k, the output signal at time $k+1$ can be predicted as:

$$\hat{y}_{k+1} = \varphi_k^T \hat{\theta}_k \tag{6}$$

Then, the *a priori* prediction error is defined as the error between the measured output and the predicted output:

$$e_{k+1} = y_{k+1} - \hat{y}_{k+1} = w_{k+1} + \varphi_k^T(\theta_k^* - \hat{\theta}_k) \tag{7}$$

In the case of the KVG model (cf. eq. (3)):

$$\varphi_k^T = (p_k \ \ v_k) \tag{8}$$

$$\theta_k^{*T} = (K_k \ \ B_k) \tag{9}$$

$$y_k = f_k \tag{10}$$

$$\hat{y}_k = \hat{f}_k \tag{11}$$

2.2.2. Robust Recursive Least Squares

The Recursive Least Squares (RLS) algorithm is probably the most widely used technique for online estimation. It was chosen in preferance to the Least Mean Square (LMS) algorithm since it is particularly efficient at estimating multi-parameter models with fast variations.

The basic RLS algorithm can be written as:

$$\hat{\theta}_k = \hat{\theta}_{k-1} + \frac{F_{k-1}\varphi_{k-1}e_k}{\frac{1}{\alpha_{k-1}} + \varphi_{k-1}^T F_{k-1}\varphi_{k-1}} \tag{12}$$

$$F_k = F_{k-1} - \frac{F_{k-1}\varphi_{k-1}\varphi_{k-1}^T F_{k-1}}{\frac{1}{\alpha_{k-1}} + \varphi_{k-1}^T F_{k-1}\varphi_{k-1}} \tag{13}$$

where α_k is a weighting function and F_k a recursively adapted covariance gain matrix, with $F_0 = F_0^T > 0$. In the basic RLS algorithm $\alpha_k = 1$, but it can also be chosen in order to normalize the prediction signal amplitude (Goodwin and Sin 1984):

$$\alpha_k = \frac{1}{1 + \varphi^T \beta \varphi} \tag{14}$$

with $\beta > 0$.

Additionally to the standard algorithm, it is recommended to use a dead-zone function (de Mathelin 2001; Ioannou and Sun 1996), so that the estimation may remain robust to noise when the absolute value of the prediction error signal is under a given threshold value. This threshold value is denoted by N_0 and chosen such that $N_0 > \nu_0$, where ν_0 is a bound on the

magnitude of the noise signal w_k. The resulting algorithm is then obtained by premultiplying F_k by $\delta(e_k)$, with:

$$\delta(e_k) = \begin{cases} 1, & \text{if } |e_k| \geq 2N_0 \\ \frac{|e_k|}{N_0} - 1, & \text{if } N_0 \leq |e_k| < 2N_0 \\ 0, & \text{if } |e_k| < N_0 \end{cases} \quad (15)$$

When the prediction error is small, a noticeable robustness improvement results.

The fact that the gain matrix F_k is not constant has some influence on the estimation of varying parameters. A persisting excitation condition on the regression vector, i.e. a sufficient level of richness of the input signals, is required for convergence of the parameters estimates to their true values when those are constant. However, the convergence of the algorithm causes the decrease of F_k to zero and the estimated parameters no longer vary, so that estimation of time-varying parameters is not possible. The RLS algorithm with covariance resetting (RLS-CR) solves the problem of the decrease of the adaption gain by resetting the covariance gain matrix F_k (Goodwin and Sin 1984). This resetting is performed at time k_r with:

$$\{k_r\} = \{k | \lambda_{min}(F_k) \leq \alpha_0^{-1} \leq \lambda_{min}(F_{k-1})\} \quad (16)$$

with $\lambda_{min}(F_k)$ the minimal eigenvalue of matrix F_k and $0 < \alpha_0^{-1} I < F_0$. To reduce the computing complexity of k_r, an equivalent condition on the trace of the covariance matrix can be used:

$$\{k_r\} = \{k | x_k = tr(F_k^{-1}) \geq \alpha_0 > tr(F_0^{-1})\} \quad (17)$$

Actually, it was shown (Goodwin and Sin 1984) that x_k can be computed recursively by:

$$x_k = x_{k-1} + \alpha_{k-1} \varphi_{k-1}^T \varphi_{k-1} \quad (18)$$

The resetting, at the time k_r, is then achieved by setting $F_{k_r} = F_0$, which also implies $x_{k_r} = x_0 = tr(F_0^{-1})$.

3. Experiments

3.1. Experimental Setup

To evaluate our estimation techniques in the context of needle insertion the following setup has been built. A PHANToM 1.5/6DOF haptic device from Sensable Technologies is used as an instrumented passive needle holder. The PHANToM end effector is equipped with an ATI Nano17 6 axis force sensor. A needle holder is mounted on the force sensor, so that needles of different size can be attached. This dedicated interface is presented in Figure 2. The PHANToM encoders are used to measure the motions of the needle during the insertions. Measurements are acquired at 1 kHz frequency rate, under real-time constraints imposed by the software implemented on Linux RTAI operating system.

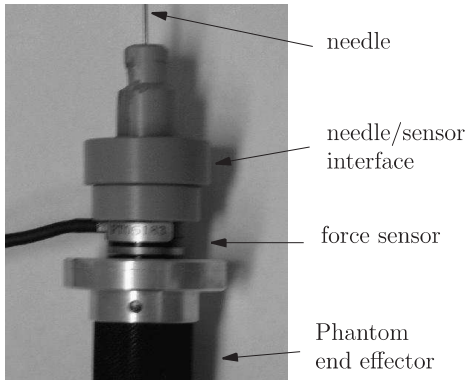

Fig. 2. Instrumented needle.

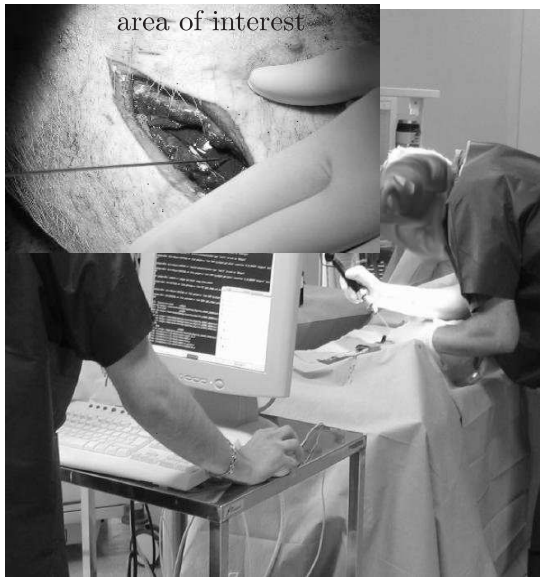

Fig. 3. Needle insertion procedure.

Since the velocity of the needle is generally very small during an intervention, given the fact that the velocity measurement is derived from position incremental encoders, it is corrupted by a large quantization noise. Estimation of the velocity has been obtained by a Kalman filter (Belanger 1992), in order to reduce the modeling error induced by the noise.

3.2. Needle Insertion Experiments

Experiments were performed *in vivo* in operating conditions as pictured in Figure 3. Needle insertions in the liver of anesthetized pigs were used as benchmarks for two reasons:

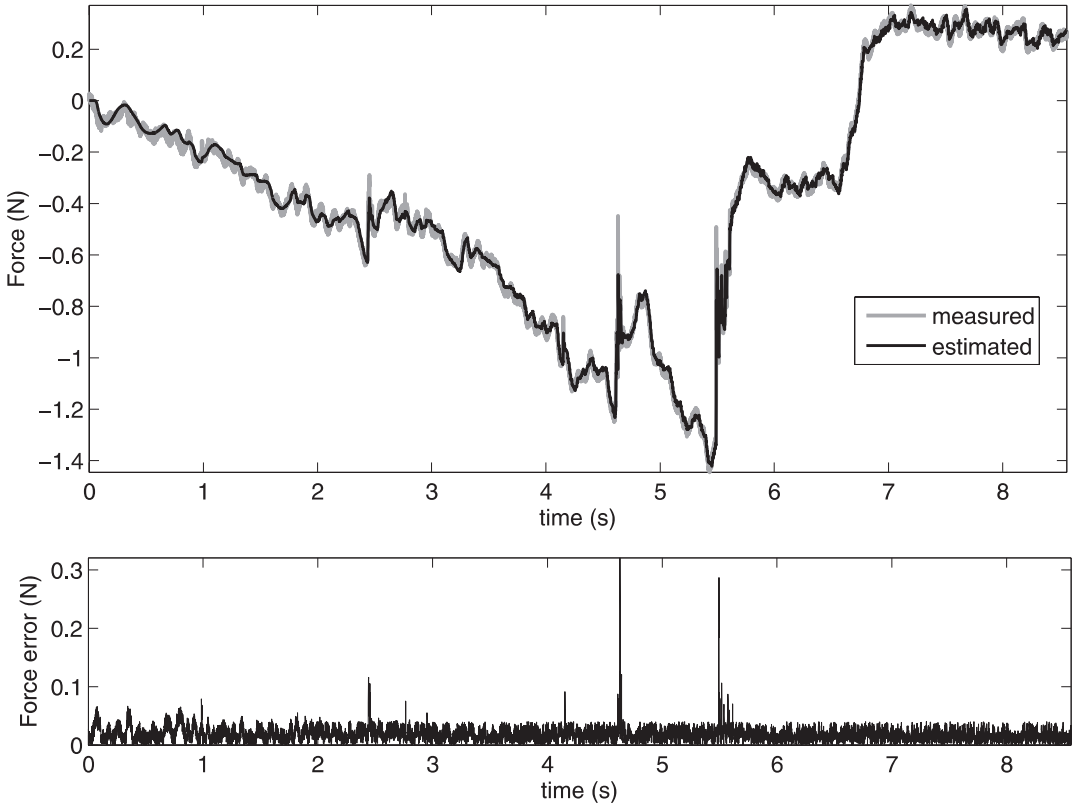

Fig. 4. Measured versus estimated force and associated absolute value of force error for the KVG model – direct access.

- the abdominal tissues of a young pig are rather similar to human tissues;
- *in vivo* properties of the tissues are much more realistic than *ex vivo* measurements because of the blood irrigation, which considerably influences the mechanical properties of the tissues, especially with the liver.

The insertion was done through a small incision on the epidermis (a new one each time), as usual in interventional radiology. The insertion was then performed through the dermis, the fat and the muscle to finally access the liver. The force reconstruction during the whole procedure was based on the estimation of the KVG model by the RLS-CR method.

3.2.1. Needle insertion into the liver with direct access

The results obtained in the case of direct access to the liver are represented in Figure 4. The first plot is a comparison between the raw measurement of the force and its reconstruction by the online RLS estimation algorithm. The second plot corresponds to the absolute value of the prediction error. The mean value of the absolute error is 0.019 N for a force amplitude ranging from -1.45 N to 0.37 N. Its standard deviation is 0.0136 N, which is relatively low. Nevertheless, during the most rapid transitions in the force measurement a transient error up to 0.32 N can be observed. This is the case of the puncture of the hepatic capsule that occurs at $t = 4.6$ s. The other two peaks observed in the error signal correspond to other nonlinearities observed during the insertion, typically the rupture of small vessels. The evolutions of the estimated parameters of the KVG model during the needle insertion are represented in Figure 5. The discontinuity due to the liver puncture clearly appears in the liver stiffness parameter, at $t = 4.6$ s.

In the case of direct insertion in the liver, the influence of the parameter $B(p,\ v,\ t)$ is limited and the reconstruction of the force obtained for a model $f(t) = -K(p,\ v,\ t)p(t)$ is quite satisfactory. In this case, the mean value of the prediction absolute error is 0.0612 N, compared to 0.019 N previously and the standard deviation is 0.041 N, compared to 0.0136 N previously. This can be explained by the low viscosity of the interaction between the needle and the liver. Therefore, as the needle tip velocity is relatively low, the contribution of the viscous force to the whole effort is relatively negligible in this type of insertion.

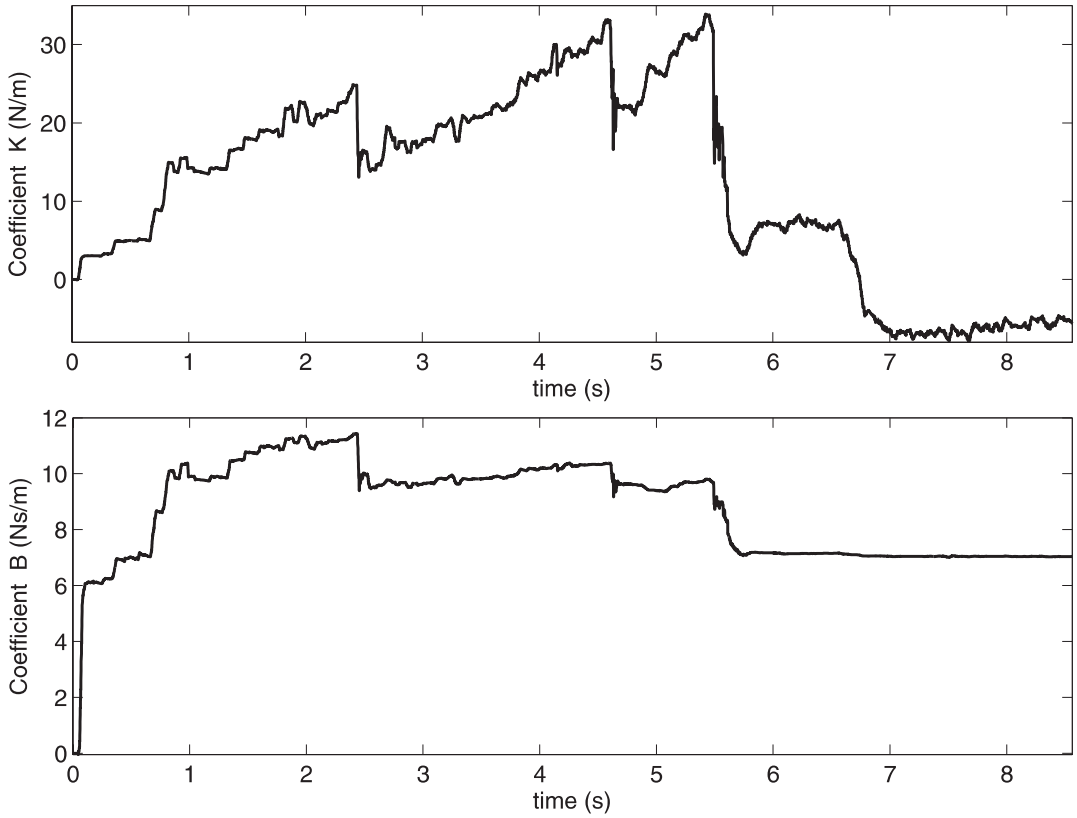

Fig. 5. Estimated parameters evolution for the KVG model – direct access.

3.2.2. Needle insertion into the liver through the skin

The results obtained in minimally invasive conditions are represented in Figure 6. The mean value of the absolute error is 0.0486 N for a force amplitude ranging from −5.69 N to 2.45 N. Its standard deviation is 0.056 N. The amplitude of the measured force is higher than in the previous case. This emphasizes the fact that most of the forces that the physician feels while inserting a needle are due to the skin, the fat and the muscles.

The most interesting results come from the model parameters analysis. The evolutions of the estimated parameters of the KVG model are represented in Figure 7. Both parameters are discontinuous because of the rupture of the successive perforated tissues. Nevertheless, one can remark that they are bounded and slowly varying, except during transitions phases. This will be used in the following section to characterize these transitions in a robust manner.

4. Detection of Force Transitions

During needle insertion, the perception of the transitions between the tissues gives haptic clues to the physician. In particular, during the time between two successive image acquisitions, it gives him some partial knowledge on where the tip of the needle is located.

This section describes a method to automatically detect the abrupt changes which characterize these transitions. The proposed method uses fault detection techniques. While initially developed in order to supervise industrial processes (Isermann 1984), fault detection is now used in several other domains (Basseville and Nikiforov 1993; Gustafsson 2000; Isermann 1993), like navigation (Nikiforov and Kireichikov 1991), seismography (Tjostheim 1975) or medical diagnosis (Corge and Puech 1986).

In the following, it is first shown that direct filtering of force measurements is not the best way to ensure the robust detection of transitions. Then, generalities about statistical fault detection methods are presented. The residual signal, which is used to build a decision function from the force estimates, is defined. Finally, detection experiments during an *in vivo* insertion are given and commented.

4.1. Direct filtering vs. fault detection

The force estimation scheme proposed in sections 2 and 3 was initially developed to characterize needle insertions. It is well

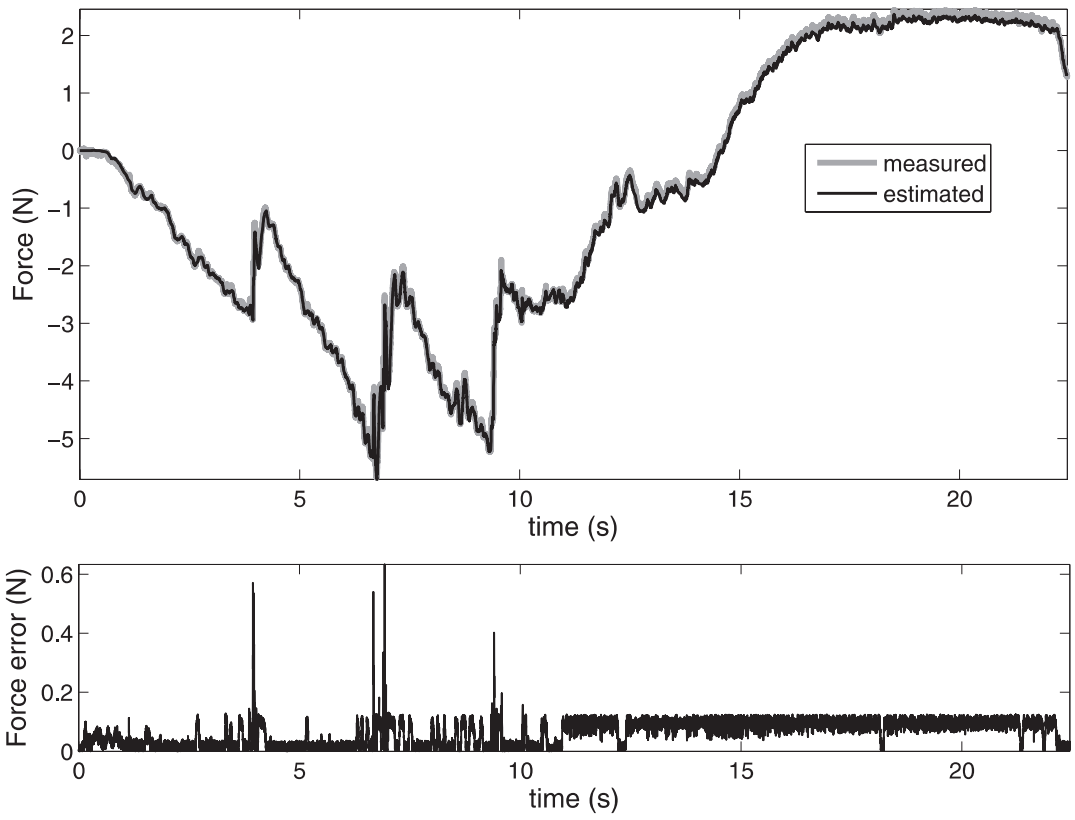

Fig. 6. Measured versus estimated force and associated absolute value of a priori prediction error for the KVG model – through the skin.

adapted to provide a physical interpretation to the interactions. However, one could wonder if ruptures or transitions should be detected from parameter variations (fault detection approach) or directly from force measurements filtering (direct filtering approach). The aim of this paragraph is to explain why standard filtering is not an efficient way to automatically detect these events.

To illustrate this discussion, consider the evolution of the force in Figure 8. It corresponds to the insertion of a needle into a liver, through the skin. It exhibits several characteristic ruptures at the interface between the different tissue layers. Two transitions are visible, at $t = 5.52$ s. and $t = 8.85$ s. The variation which can be observed at $t = 14.5$ s. is relatively sudden and could be considered as a membrane rupture without some expertise. However, it does not correspond to a transition, but to the fast needle extraction. So, good experimental detection results would consist in the detection of the first two events alone.

To detect fast transitions in the force signal, we can first evaluate the norm of the derivative of the force measurement, i.e. $(f_k - f_{k-1})^2$. The signal derivative is a very simple form of high-pass filtering, which has the advantage that no parameter tuning is needed, except threshold values for the detection of significant transient. The design of a more elaborate high-pass filter is also possible. However, it would require the selection of several parameters (e.g. cut-off frequency) that cannot easily be deduced from the force signal itself. Whatever the selection, the detection associated to high-pass filtering will suffer from high frequency amplification. Figure 9 represents $(f_k - f_{k-1})^2$ when force measurements are noisy. The noise that has been added to the force signal corresponds to a commercial 1 DOF Scaime force cell (Scaime 2006). It can be considered as a white noise with a variance of $6.25 \cdot 10^{-4}$ N^2, added to the force signal of Figure 8. As can be observed, noise has a noticeable effect on the detection of the ruptures. The selection of an adapted threshold value in order to detect the two ruptures would be very difficult with such noisy measurements. Band-pass filtering would certainly be a more efficient choice, in terms of filtering. However, the number of parameters to empirically tune would make the approach impractical. Therefore, a statistical fault detection approach known for its robustness is preferred in the following section.

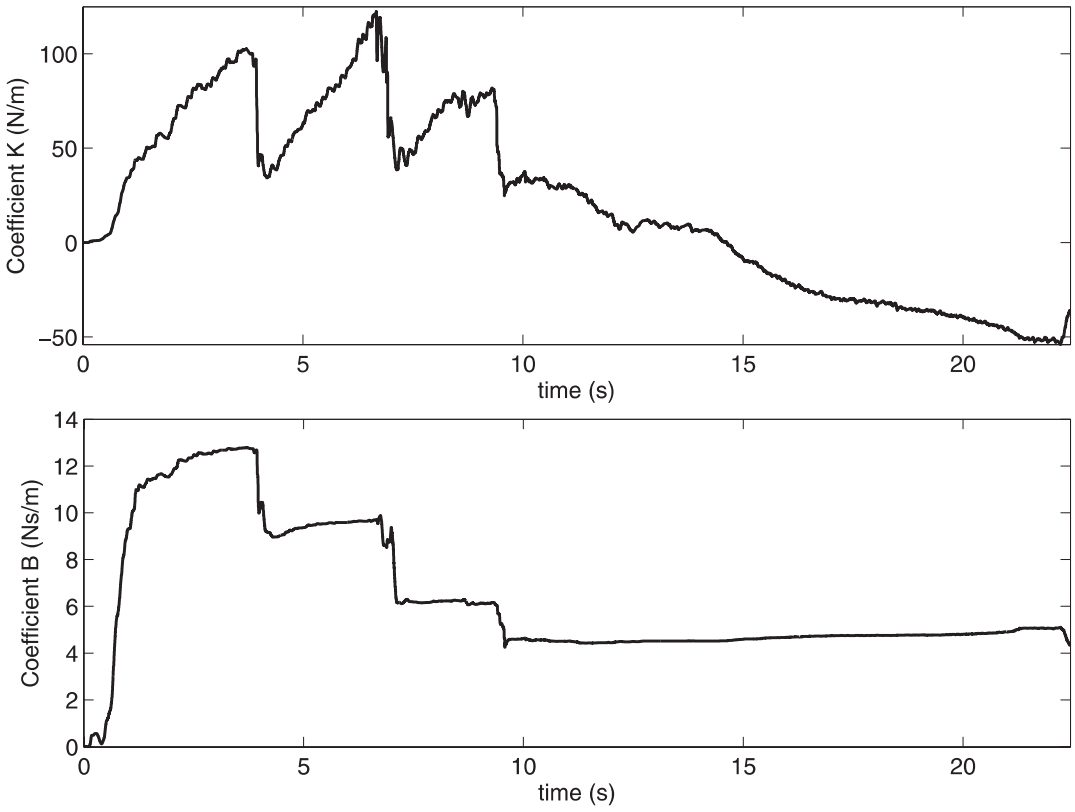

Fig. 7. Estimated parameters evolution for the KVG model – through the skin.

4.2. Automatic Rupture Detection

Statistical methods are among the most popular techniques to diagnose fast variations of mean value or variance. They are based on the analysis of a random signal, generally called residual and denoted by ε_k, with a probability density $p_\psi(\varepsilon_k)$. The residual probability distribution is known before a change happens. A change (or a fault) corresponds to a new probability distribution. Parameter ψ either corresponds to the mean value or to the variance of the residual, which varies from ψ_0 to ψ_1 at the fault detection time. Abrupt changes are then characterized by the following statistical hypothesis:

$$\begin{cases} \mathcal{A}_0 & : \quad \psi = \psi_0 \quad \text{if no change occurs} \\ \mathcal{A}_1 & : \quad \psi = \psi_1 \quad \text{if there is a change} \end{cases} \tag{19}$$

With these assumptions, fault detection consists of verifying whether the residual sample at time k matches $\mathcal{A}_0$ or $\mathcal{A}_1$. The algorithm uses a distance measurement s_k which is generally built from the log-likelihood ratio:

$$s_k = \ln \frac{p_{\psi_1}(\varepsilon_k)}{p_{\psi_0}(\varepsilon_k)} \tag{20}$$

4.3. Residual Generation

The purpose of residual generation is to build a new signal with maximum richness regardless of changes. In the ideal case, the residual is zero before the change and different from zero afterwards. In practice, modeling errors, disturbances or measurement noise are limitations to these ideal conditions. Generally, the residual is viewed as a white noise during the phases without changes, where the mean value or the variance is known and do not vary a lot. Thus, the residual signal is built to follow a Gaussian distribution of mean value m and variance σ^2, i.e. with a probability density:

$$p_\psi(\varepsilon_k) = \frac{1}{\sigma\sqrt{2\pi}} e^{\frac{-(\varepsilon_k - m)^2}{2\sigma^2}} \quad \text{with} \quad \psi = \{m, \sigma\} \tag{21}$$

The detection of changes then amounts to checking, for each residual sample, if it verifies the hypothesis of whiteness of the signal.

Traditionally, residuals are generated from a model of the system. In our case, we naturally define the residual signal from the estimate of the parametric model previously presented. In our case, the insertion force is estimated online, as represented in Figure 10. It is natural to select the prediction

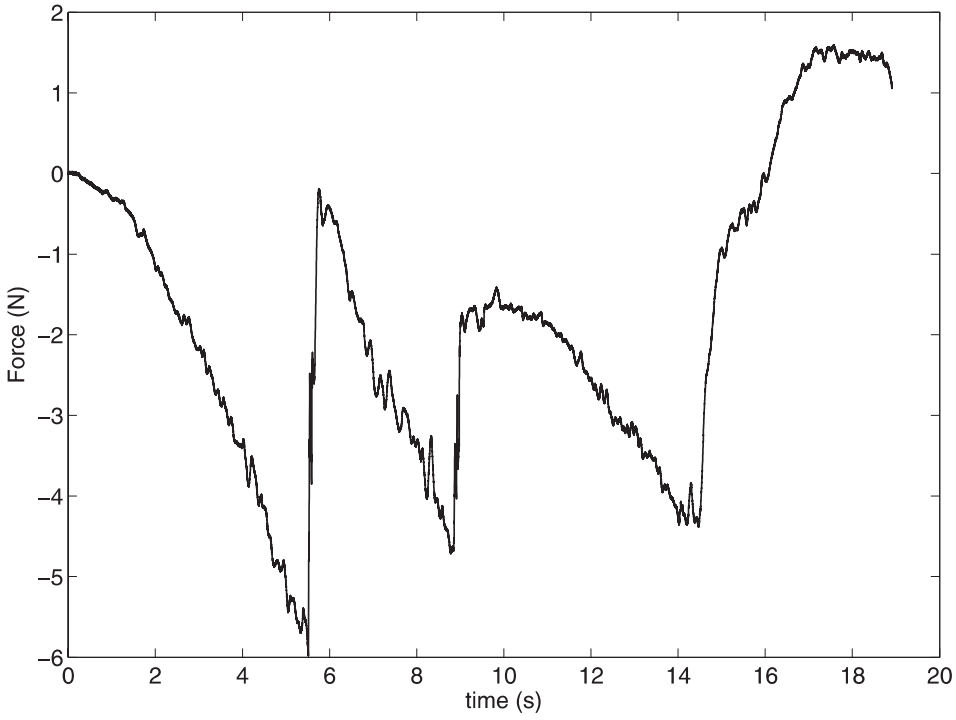

Fig. 8. Evolution of the insertion forces used for the detection experiments.

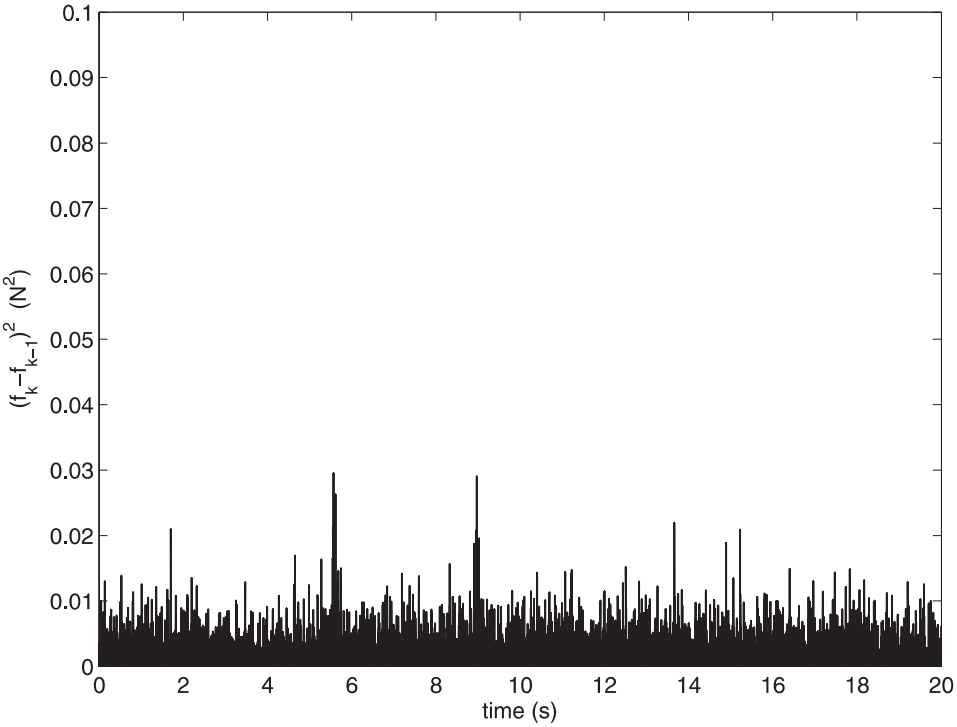

Fig. 9. Detection of fast transitions with high-pass filtering for a measured force with noise.

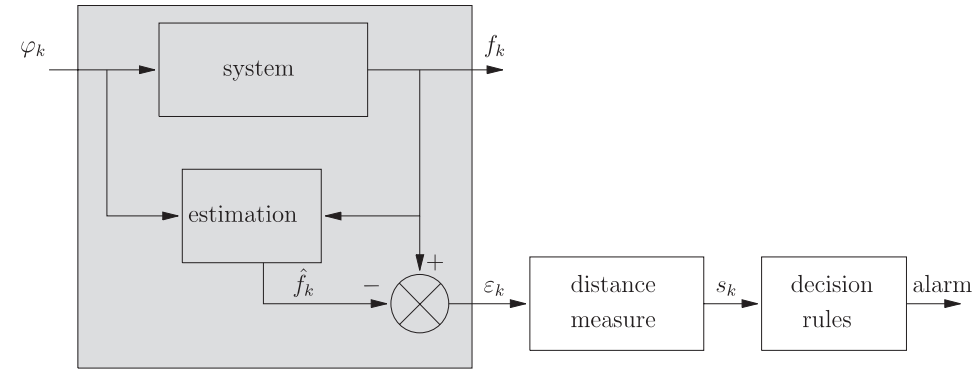

Fig. 10. Detection principle with model estimation.

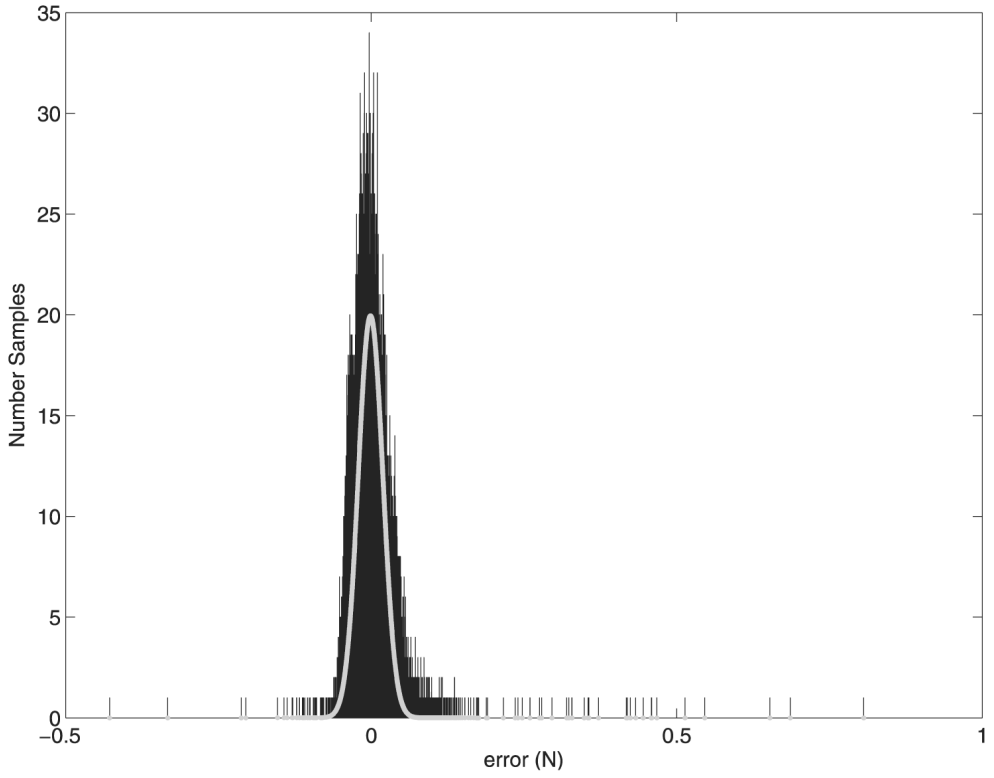

Fig. 11. Prediction error distribution and Gaussian centered distribution model with variance σ_0^2 in the absence of sudden changes during an insertion.

error as the residual, i.e. $\varepsilon_k = e_k$, since its value is close to zero as long as the parameters vary slowly, and suddenly changes at the time of fast parameter variations.

Using a stationarity and ergodicity assumption, the probability distribution of the prediction error e_k is represented in Figure 11, in the case of needle insertion without rupture. As can be observed, it has a Gaussian distribution as long as the parameters vary slowly. It can be seen that the mean value is equal to zero. The measured residual variance under assumption $\mathcal{A}_0$ is $\sigma_0^2 = 4 \cdot 10^{-4}$ N^2.

4.4. Distance Measurements

There are two faults categories: additive faults and non-additive faults, also called multiplicative faults. Additive faults

are generally due to actuator or sensor failures and correspond to a discontinuity in the measured signals. Non-additive faults are due to a fast change in the nominal behavior of the system, and their detection is difficult. Concerning needle insertion, both approaches can be considered. Indeed, ruptures in the force signal during an insertion can be seen either as a change in the system model, i.e. a stiffness abrupt variation accounting for a membrane rupture or as a force sensor failure.

4.4.1. Distance measurements for additive faults

Mean value changes If it is considered that the changes only affect the mean value of the signal, then $\psi = m$. If the mean value is m_0 before the change and if a significant change is characterized by a new mean value m_1, then, from equations (20) and (21):

$$s_k = \frac{m_1 - m_0}{\sigma^2}\left(\varepsilon_k - \frac{m_0 + m_1}{2}\right) \tag{22}$$

If σ and m_1 are known and if $m_0 = 0$, then (22) can be simplified and we can simply select $s_k = \varepsilon_k$ (Gustafsson 2000).

Variance changes If it is considered that the changes only affect the variance, then $\psi = \sigma^2$. If the variance is σ_0^2 before the change and σ_1^2 afterwards, m being constant, then, from (20) and (21):

$$s_k = \ln\frac{\sigma_0}{\sigma_1} + \left(\frac{1}{\sigma_0^2} - \frac{1}{\sigma_1^2}\right)\frac{(\varepsilon_k - m)^2}{2} \tag{23}$$

If σ_0 and σ_1 are known and $m = 0$, then we can simply select $s_k = \varepsilon_k^2$ (Gustafsson 2000).

4.4.2. Distance measurements for multiplicative faults

In this case, the purpose is to detect the fast variations or the nonlinearities which affect each parameter independently. As already mentioned, the model parameters vary in time and with position of the needle. As the model estimate is valid only if the parameters vary slowly, then we can make the assumption that the difference between two samples of the estimated parameters has a Gaussian centered distribution with a given variance. As soon as the parameter variations do not verify this hypothesis, a change is detected. The recursive estimation algorithm directly gives us this information since:

$$\hat{\theta}_k = \hat{\theta}_{k-1} + H_k \tag{24}$$

with, from equation (12):

$$H_k = \frac{F_{k-1}\varphi_{k-1}e_k}{\frac{1}{\alpha_{k-1}} + \varphi_{k-1}^T F_{k-1}\varphi_{k-1}} \tag{25}$$

As H_k depends on the prediction error, which is assumed to have a Gaussian distribution during normal phases, it is possible to define:

$$s_k = H_k \tag{26}$$

with $s_k \in \mathbb{R}^n$, $n = \dim(\hat{\theta}_k)$.

4.4.3. Choice of the distance measurement for needle insertion

For the detection of ruptures during needle insertions, it was initially proposed in (Barbé et al. 2006) to use the distance measurement of eq. (26): $s_k = H_k$. Nevertheless, even if the corresponding detection is satisfactory, the choice of the threshold value to decide between hypothesis $\mathcal{A}_0$ and $\mathcal{A}_1$ is rather difficult in this case. Indeed, it is not easy to foresee the range of the parameter variations that may be detected from H_k.

On the contrary, the occurrence of sudden changes corresponds to an increase of the prediction error until the estimation algorithm converges again. This can efficiently be correlated to variance changes. Because of the Gaussian distribution of the residuals as shown in Figure 11, the tissue transitions that correspond to large variations of the prediction error can efficiently be detected by the variation of the prediction error variance. Therefore, in the following, we will use $\varepsilon_k = e_k$ as the residuals and $s_k = \varepsilon_k^2$ as the distance measurement. From the residual density of probability characteristics as illustrated in Figure 11, we can choose the threshold value corresponding to the variance change detection.

To emphasize the robustness properties of the method we present in Figure 12 the evolution of the distance measurement resulting from the force reconstruction of the signal plotted in Figure 8 with added noise as in section 4.1. This result can be compared with the direct filtering of the force signal, presented in Figure 9. The distance measurement computed in this manner is less corrupted by noise than previously observed with direct high-pass filtering. The two abrupt changes that have to be detected now correspond to two very distinct peaks in the distance measurement, in contrast to what was obtained in Figure 9.

4.5. Detection Algorithm

The final step consists in deciding when hypothesis $\mathcal{A}_0$ or $\mathcal{A}_1$ applies. This is done with the CUSUM algorithm.

CUSUM algorithm The application of the CUSUM algorithm (Page 1954) is based on the fact that the mean value of s_k changes when a change of hypothesis occurs. The detection of a significant change is decided when a decision function g_k is greater than a chosen threshold value, denoted by γ. A typical decision function is defined by:

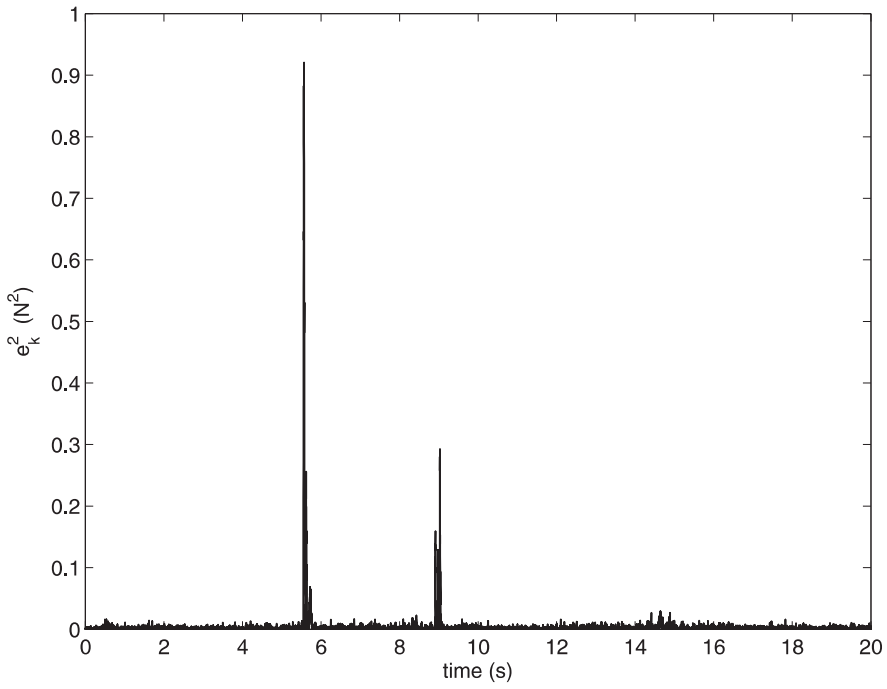

Fig. 12. Distance measurement computed from the prediction error on the force for a measured force with noise.

$$\begin{cases} g_0 &= 0 \\ g_k &= \max\left(g_{k-1} + s_k - \nu, 0\right) \end{cases} \tag{27}$$

where ν is the drift parameter of the mean value of s_k, usually selected equal to half of the amplitude of the change being detected (Basseville and Nikiforov 1993; Gustafsson 2000).

Detection threshold tuning The time delay between the effective time instant of detection and the true event depends directly on the choice of the threshold value γ. A bad choice is likely to lead to detection mistakes: no detection in the case of a too large threshold or wrong detections in the case of a too small threshold. In our experiments, this threshold was tuned in an empirical way, in order to correctly detect events that were identified based on expertise. However, automatic adjustment of an optimal detection threshold is possible, at the expense of relatively complex techniques, which are not developed in this article. For more details, the reader is referred to (Basseville and Nikiforov 1993).

4.6. Application to Rupture Detection During Needle Insertion

The estimated variances from experiments were $\sigma_0^2 = 4 \cdot 10^{-4}$ N^2 and $\sigma_1^2 \geq 4 \cdot 10^{-2}$ N^2 during transient phases. Therefore, to detect changes in the variance from σ_0^2 to σ_1^2, we choose $\gamma = \frac{\sigma_1^2 - \sigma_0^2}{2} = 1.98 \cdot 10^{-2}$ N^2 and $\nu = \frac{\sigma_1^2 + \sigma_0^2}{2} = 2.02 \cdot 10^{-2}$ N^2. Then, for the insertion described, the evolution of the decision function is given at the top of Figure 13. The time instants of change detection are represented at the bottom of Figure 13. The signal is zero over the time horizon considered, except when the two changes are detected. This confirms that the detection function and the detection threshold choices are suitable.

As illustrated in the previous section, the algorithm allows one to properly detect the two force ruptures. The true event moments occur at $t = 5.22$ s and $t = 8.85$ s. The detections occur at $t = 5.52$ s and $t = 8.86$ s. We can see that the detection delay is always less than 10 ms. We also notice that the second detection is more delayed than the first one, partly because the second rupture is less sudden. This might be due to the way the needle was inserted or to the physician's handling of the needle when the rupture happened. In conclusion, the algorithm remains accurate and fast, even when the change in the force profile is not a sudden rupture.

5. Applications of Rupture Detection to Event-based Teleoperation

As underlined in the introduction, the haptic clues that the practitioner feels during needle insertions are very important. However, it can sometimes be difficult to detect these events, in particular for physicians with a lack of training or if the force variations are not large enough. Using the detection scheme

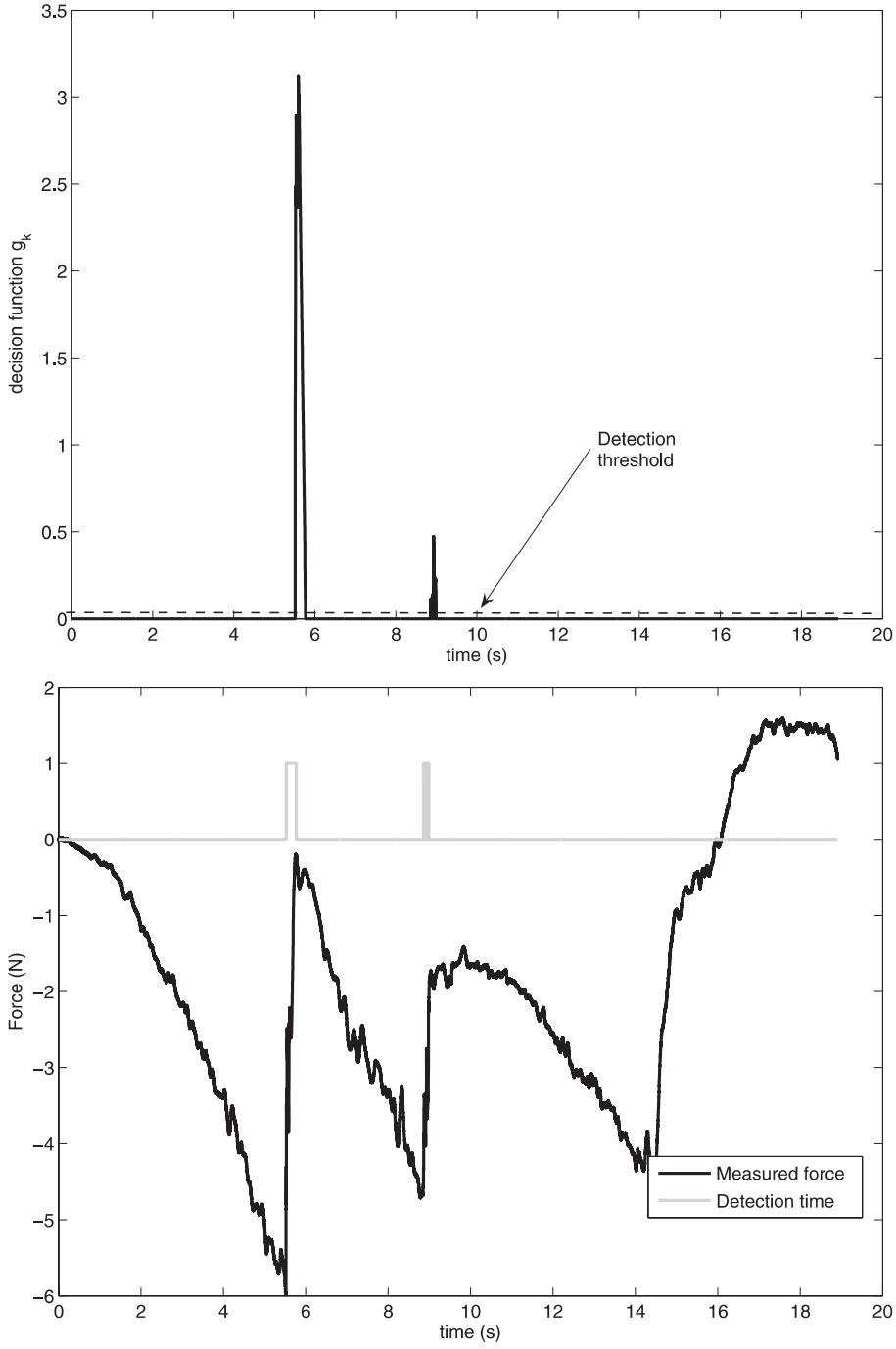

Fig. 13. Evolution of the decision function (top), of the insertion forces and the rupture detection (bottom) with the CUSUM algorithm.

presented in section 4, the haptic perception of force ruptures can be enhanced. To that purpose, the simplest solution would be to provide visual or acoustic information on the graphical user interface. Event detection can also be used for augmented force feedback.

5.1. Augmented Event-based Teleoperation

In the case of force feedback teleoperated needle insertions, the rupture perception would require very fast transient response time. However, due to the classical stability versus per-

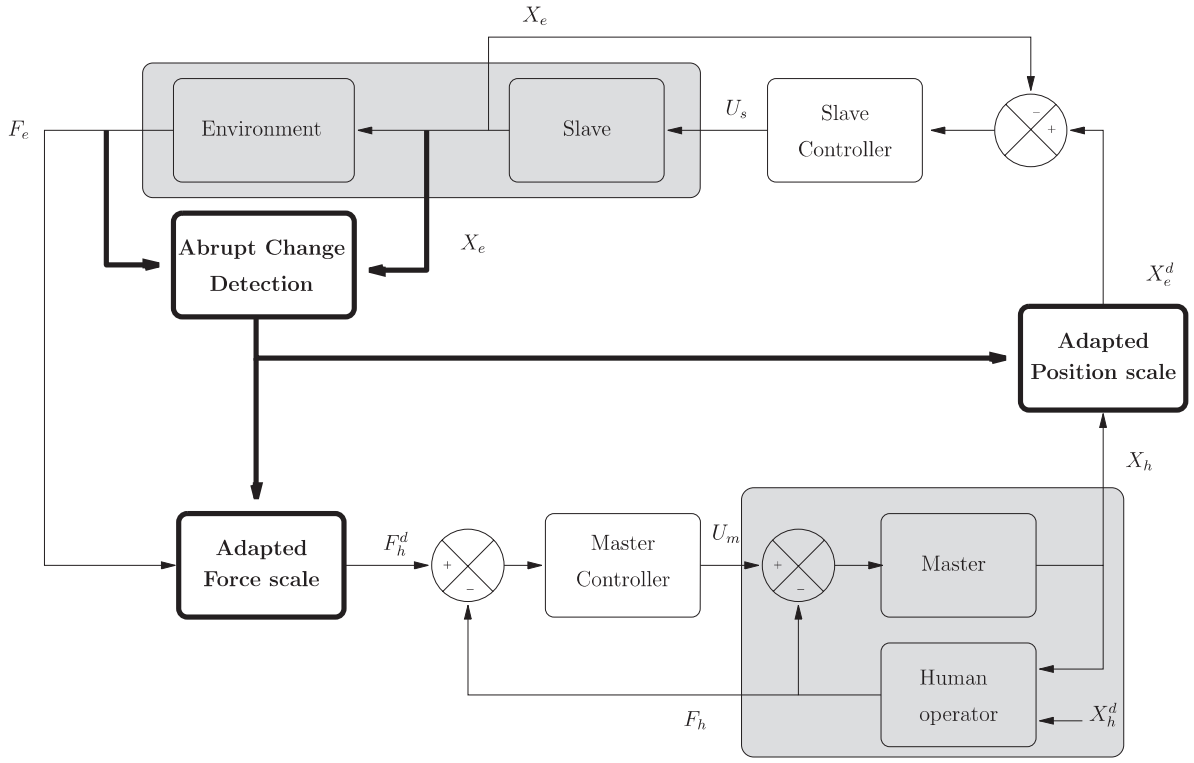

Fig. 14. Block diagram of the modified force–position controller, with transient adaptation in bold.

formance trade-off, the performance of a bilateral controller are often limited to guarantee the unconditional stability of the system. To cope with this problem, rupture detection can be used to temporarily augment the force feedback during these phases. To illustrate this proposition, consider the modified force–position control scheme represented in Figure 14. In the classical bilateral force–position teleoperation scheme (Hannaford 1989), the position X_h of the master manipulator serves as the reference for the slave manipulator and the measured interaction force F_e between the slave manipulator and the environment is fed back to the human operator through the master manipulator. The desired motion of the human is represented by X_h^d. The position and the force sent from one side to the other side are usually scaled by a constant factor.

The modification in Figure 14 consists in temporarily adapting the scale factors when an abrupt change is detected. This event-based haptic augmentation is somehow comparable to the work of Kuchenbecker et al. (2006), which uses an event-based strategy to augment force realism in contact with stiff surfaces. In our application, we use the following strategy to react to the ruptures that occur during needle interactions:

- when an abrupt change detection occurs, the reference force applied to the master manipulator is modified during a short period of time in order to increase the variation of forces;
- simultaneously, the slave position is frozen to avoid an excessive penetration of the needle that may occur just after the rupture of the tissue.

The rendering will then be voluntarily exaggerated, but in a transient and soft manner. This temporary adaptation of the control may not be associated to stability problems if the local slave control loop is stable and if the local master control loop with the human operator is stable, as is usually the case. Indeed, on the one hand the slave position is frozen during the augmentation phase, so that the global feedback loop is temporarily open. On the other hand, the local loops are stable and the augmented force signal F_h^d is a bounded exogenous input to the local master loop. The augmented force signal is computed in order to be continuous, thus allowing a smooth haptic perception. Of course, special care should be taken when exiting the augmented mode in order to avoid immediate switching back, for example, by adding a simple hysteresis on the decision function. A complete stability analysis would require hybrid modelling, taking into account the exact switching control law, which is beyond the scope of this article.

5.2. Simulations

First, we simulated teleoperated needle insertions with a classical force-position control scheme. We tuned the teleoperation

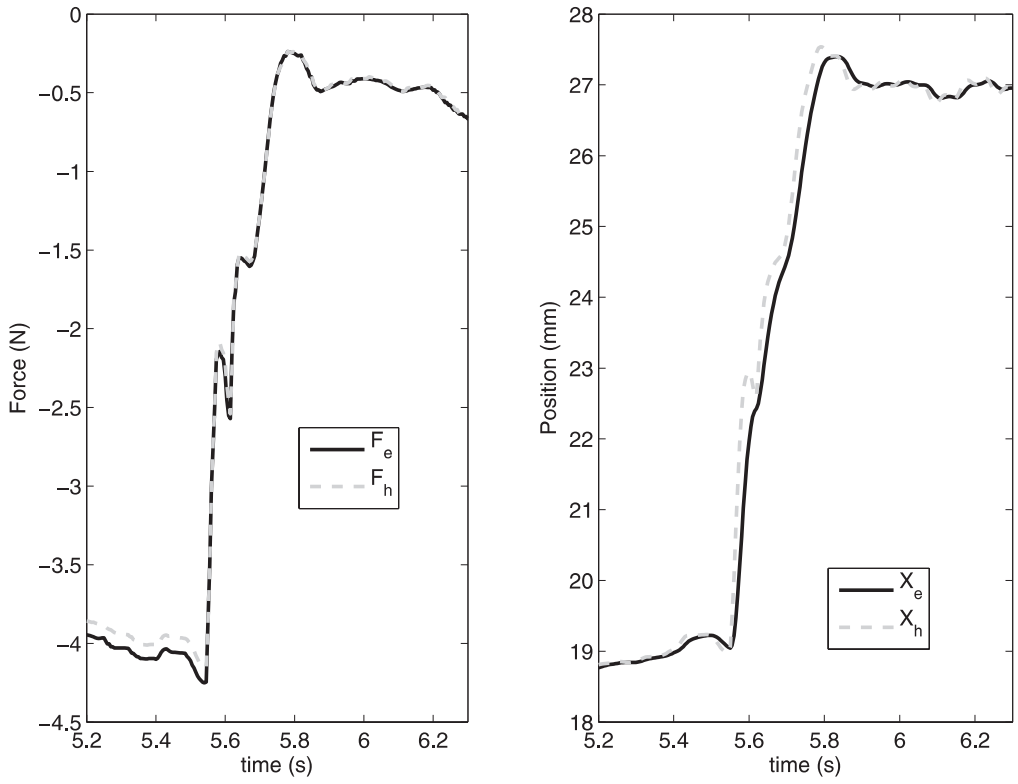

Fig. 15. Master and slave forces (left) and positions (right) with classical force-position teleoperation scheme.

control so that the simulated teleoperation system may remain stable and as transparent as possible (Lawrence 1993), during standard interactions with soft tissues. The model used for the simulation are given in the appendix A. *In vivo* measured data were used to provide position and velocity references to the master and interaction forces to the slave. The data considered correspond to a temporal window around the first rupture detected in Figure 13. Figure 15 represents the forces and positions of the master and the slave manipulators. The system exhibits good tracking performance, even during this rupture. However, because of the discontinuity in the force profile, we can verify that the user inserts the needle in the tissue very quickly: the slave position jumps from 9 mm in approximately 300 ms. Such an excessive penetration can of course be dangerous for the patient if it is not anticipated.

Now consider the event-based strategy to limit this undesirable penetration and to enhance force variations during the rupture. The results obtained for the same data and the same system, with the modified force–position control scheme, are presented in Figure 16. The transition corresponding to the needle puncture lasts approximately 0.5 s. and is indicated by the detection time plot. During this phase, the force F_h^d fed back to the user is temporarily adjusted so as to converge faster to zero than with the classical scheme. This more abrupt variation will augment the perception of discontinuity. The position profile exhibits good tracking performances in the absence of ruptures. During the transition phase, the slave manipulator position is frozen while the master manipulator position jumps from 19 mm to 28 mm. This approach provides a teleoperation scheme for needle insertion safer than the classical scheme.

6. Conclusion

In this paper we have presented the results of *in vivo* needle insertion experiments. The behavior of tissue has been characterized during percutaneous interventions on a living animal. Recordings of typical force profiles with respect to needle tip depth and velocity were obtained. From the analysis of these data, we believe that accurate biomechanical models cannot be estimated online. For this reason, we have chosen a simple two parameters model to relate forces on the needle to its tip position and velocity. In these conditions, the corresponding model has varying parameters, which can be estimated online by a recursive least square algorithm with covariance resetting and a dead-zone.

From this model estimation we have developed a method to detect changes in the model and correlate them to the membrane ruptures that occur during needle insertions. The proposed method, which is based on fault detection techniques,

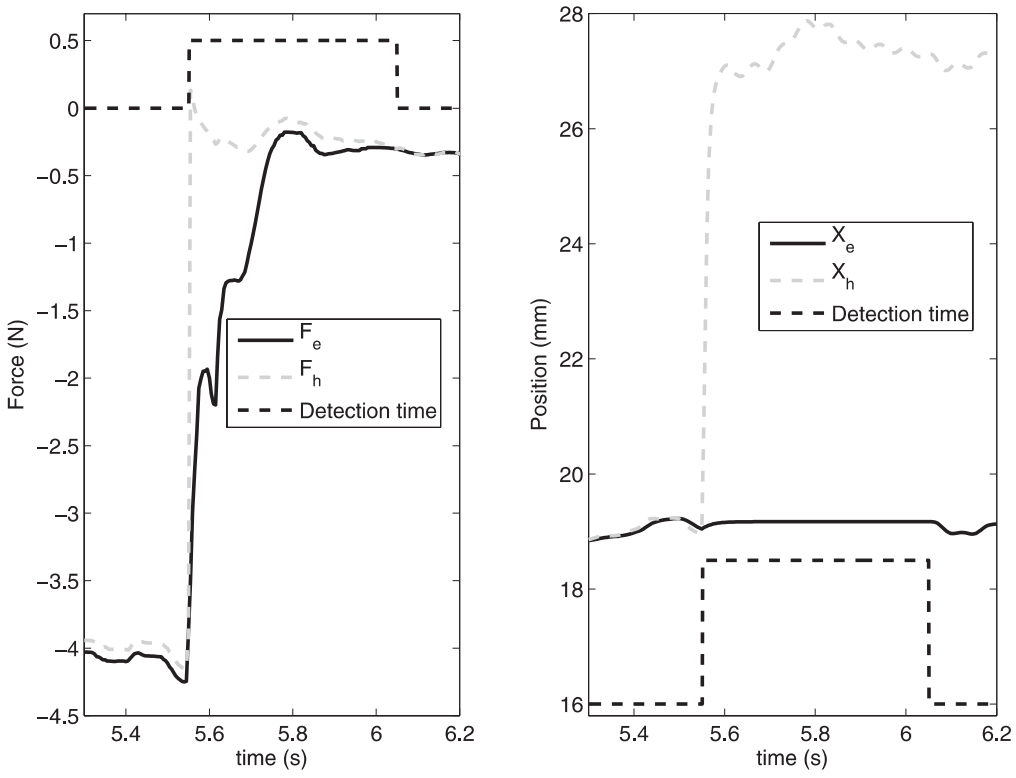

Fig. 16. Master and slave forces (left) and positions (right) with the modified force-position teleoperation scheme.

gives very good performances regardless to robustness and detection time.

Finally, we discussed the possible applications of rupture detection to assist percutaneous procedures, with a focus on augmented teleoperation. We proposed a simulation to show that force rupture perception can be augmented by providing to the master user more rapid transient responses or by preventing insecure fast motions that may occur after membrane piercing.

Concerning needle insertion modeling, a possible extension of this work is to incorporate friction terms in the estimated model. Further developments also include experimentation of the proposed directions in augmented teleoperation. Finally, the exploitation of this work in the context of a force feedback teleoperated needle driver with *in vivo* validations is the ultimate objective of this project.

Appendix – Simulation Model

The transfer functions of the models and controllers used in the simulations of section 5 are:

- master:

$$G_m(s) = \frac{X_h(s)}{U_m(s)} = \frac{1}{0.245s^2 + 4.1s} \qquad (28)$$

where $U_m(s)$ is the master control;

- master controller:

$$U_m(s) = \frac{K_i^m}{s}\left(F_e(s) - F_h(s)\right) + F_e(s) \qquad (29)$$

where $K_i^m = 12$;

- slave:

$$\begin{aligned} G_s(s) &= \frac{X_e(s)}{U_s(s)} \\ &= \frac{7.778s + 656}{s^3 + 104.1s^2 + 1.131 \cdot 10^{-4}s} \end{aligned} \qquad (30)$$

where $U_s(s)$ is the slave control;

- slave controller:

$$U_s(s) = K_p^s\left(X_h(s) - X_e(s)\right) - K_v^s s X_e(s) \qquad (31)$$

where $K_p^s = 1300$ and $K_v^s = 15$;

- the user model is derived from the five-parameters model proposed by deVulgt (de Vulgt 2004):

$$F_h(s) = \frac{sZ_a(s)}{1 + Z_a(s)G_h(s)} \times \left(Z_h(s)G_h(s)X_h^d(s) - X_h(s)\right) \quad (32)$$

where:

$$Z_a(s) = \frac{k_a + b_a s}{s} \quad (33)$$

$$Z_h(s) = \frac{k_h + b_h s}{s} \quad (34)$$

$$G_h(s) = \frac{s}{m_h s^2 + b_h s + k_h} \quad (35)$$

with the numerical values $k_a = 733$ N·m^{-1}, $b_a = 37.3$ N·s·m^{-1}, $k_h = 14998$ N·m^{-1}, $b_h = 178$ N·s·m^{-1} and $m_h = 1.88$ kg.

Acknowledgements

The authors would like to thank the IRCAD/EITS staff for their help during *in vivo* experiments inside their facilities, with special thanks to Antonello Forgione and Stefano Sereno.

This work is supported by the Alsace Regional Council and the French National Center for Scientific Research (CNRS).

References

Barbé, L., Bayle, B., de Mathelin, M., and Gangi, A. (2006). Online robust model estimation and haptic clues detection during in vivo needle insertions. In *IEEE International Conference on Biomedical Robotics and Biomechatronics*, Pisa, Italy, February.

Basseville, M. and Nikiforov, I. (1993). *Detection of Abrupt Changes - Theory and Applications*. Information and System Sciences Series. Prentice Hall, Englewood Cliffs, NJ.

Belanger, P. (1992). Estimation of angular velocity and acceleration from shaft encoder measurements. In *IEEE International Conference on Robotics and Automation*, Nice, France, May.

Brett, P., Harrison, A., and Thomas, T. (2000). Schemes for the identification of tissue types and boundaries at the tool point for surgical needles. *IEEE Transactions on Information Technology in Biomedicine*, **4**(1): 30–36.

Corge, J. and Puech, F. (1986). Analyse du rythme cardiaque foetal par des méthodes de détection de ruptures. In *INRIA International Conference Analysis and optimization of Systems*, Antibes, France (in French).

De Gersem, G. (2005). *Kinaesthetic Feedback and Enhanced Sensitivity in Robotic Endoscopic Telesurgery*. PhD thesis, Catholic University of Leuven.

De Gersem, G., Van Brussel, H., and Tendick, F. (2005). Reliable and enhanced stiffness perception in soft-tissue telemanipulation. *The International Journal of Robotics Research*, **24**(10): 805–823.

de Mathelin, M. (2001). *Commande Adaptative et Applications*. Hermès Science, R. Lozano and D. Taoutaou editors, ch. Panorama des algorithmes récursifs d'estimation paramétrique (in French).

de Vulgt, E. (2004). *Identification of Spinal Reflexes*. PhD thesis, Delft University of Technology, The Netherlands.

DiMaio, S. and Salcudean, S. (2003). Needle insertion modeling and simulation. *IEEE Transactions on Robotics and Automation*, **19**(5): 864–875.

Diolaiti, N. (2005). *Robotic Interaction: Analysis and Control*. PhD thesis, Universita' di Bologna, 2005.

Diolaiti, N., Melchiorri, C., and Stramigioli, S. (2005). Contact impedance estimation for robotic systems. *IEEE Transactions on Robotics*, **21**(5): 925–935.

Fung, Y. (1993). *Biomechanics : Mechanical Properties of Living Tissues*. Springer-Verlag.

Goodwin, G. and Sin, K. (1984). *Adaptive Filtering Prediction and Control*. Information and System Sciences. Prentice-Hall.

Gustafsson, F. (2000). *Adaptive Filtering and Change Detection*. John Wiley & Sons, Ltd.

Hannaford, B. (1989). A design framework for teleoperators with kinesthetic feedback. *IEEE Transaction on Robotics and Automation*, **5**(4): 426–434.

Heverly, M., Dupont, P., and Triedman, J. (2005). Trajectory optimization for dynamic needle insertion. In *IEEE International Conference on Robotics and Automation*, Barcelona, Spain, April.

Hong, J., Dohi, T., Hashizume, M., Konishi, K., and Hata, N. (2004). An ultrasound-driven needle-insertion robot for percutaneous cholecystostomy. *Physics in Medicine and Biology*, 441–455.

Hunt, K. and Crossley, F. (1975). Coefficient of restitution interpreted as damping in vibroimpact. *ASME Journal of Applied Mechanics*, 440–445.

Ioannou, P. and Sun, J. (1996). *Robust Adaptive Control*. Prentice-Hall.

Isermann, R. (1984). Process fault detection based on modeling and estimation methods – a survey. *Automatica*, **20**: 387–404.

Isermann, R. (1993). Fault diagnosis of machines via parameter estimation and knowledge processing: tutorial paper. *Automatica*, **29**(4): 815–835.

Kobayashi, Y., J., J. O., and Fujie, M. (2004). Physical properties of the liver for needle insertion control. In *IEEE International Conference on Intelligent Robots and Systems*, Sendai, Japan, September/October.

Kronreif, G., Fürst, M., Kettenbach, J., Figl, M., and Hanel, R. (2003). Robotic guidance for percutaneous interventions. *Journal of Advanced Robotics*, **17**(6): 541–560.

Kuchenbecker, K., Fiene, J., and Niemeyer, G. (2006). Improving contact realism through event-based haptic feedback. *IEEE Transactions on Visualization and Computer Graphics*, **12**(2): 117–123.

Lawrence, D. (1993). Stability and transparency in bilateral teleoperation. *IEEE Transaction on Robotics and Automation*, **9**(5): 624–637.

Maurel, W. (1998). *3D Modeling of the Human Upper Limb including the Biomechanics of Joints, Muscles and Soft Tissues*. PhD thesis, Ecole Polytechnique Fédérale de Lausanne, Switzerland.

Maurin, B., Barbé, L., Bayle, B., Zanne, P., Gangloff, J., de Mathelin, M., Gangi, A., and Forgionne, A. (2004b). In vivo study of forces during needle insertions. In *Scientific Workshop on Medical Robotics, Navigation and Visualization*, Remagen, Germany, March.

Maurin, B., Gangloff, J., Bayle, B., de Mathelin, M., Piccin, O., Zanne, P., Doignon, C., Soler, L., and Gangi, A. (2004a). A parallel robotic system with force sensors for percutaneous procedures under CT-guidance. In *International Conference on Medical Image Computing and Computer Assisted Intervention*, Saint-Malo, France, September.

Nikiforov, I., Varavva, V., and Kireichikov, V. (1991). Application of statistical fault detection algorithms for navigation systems monitoring. In *SAFEPROCESS*, Baden-Baden, Germany.

Okamura, A., Simone, C., and O'Leary, M. (2004). Force modeling for needle insertion into soft tissue. *IEEE Transactions on Biomedical Engineering*, **51**(10): 1707–1716.

Ottensmeyer, M. and Salisbury, J. (2001). In vivo data acquisition instrument for solid organ mechanical properties. In *International Conference on Medical Image Computing and Computer Assisted Intervention*, Utrecht, The Netherlands, pp. 975–982.

Page, E. (1954). Continous inspection schemes. *Biometrika*, **41**: 100–115.

Rhim, R., Goldberg, S., Dodd, D., Solbiati, L., Lim, H., Tonolini, M., and Cho, O. (2001). Essential techniques for successful radio-frequency thermal ablation of malignant hepatic tumors. *RadioGraphics*, **21**: S17–S35.

Scaime (2006). *Miniature Force Transducer K-1107* (http://www.scaime.com).

Simone, C. and Okamura, A. (2002). Modeling of needle insertion forces for robot-assisted percutaneous therapy. In *IEEE International Conference on Robotics and Automation*, Washington DC, USA, May.

Stoianovici, D., Cadeddu, J., Demaree, R., Basile, H., Taylor, R., Whitcomb, L., and Kavoussi, L. (1997). A novel mechanical transmission applied to percutaneous renal access. *ASME Dynamic Systems and Control Division*, **61**: 401–406.

Tjostheim, D. (1975). Autoregressive representation of seismic p-wave signals with an application to the problem of short period discriminant. *Geophysical Journal Royal Astronomical Society*, **43**(2): 269–291.

Washio, T. and Chinzei, K. (2004). Needle force sensor, robust, sensitive detection of the instant of needle puncture. In *International Conference on Medical Image Computing and Computer-Assisted Intervention*, Saint-Malo, France, September.

Yen, P.-L., Hibberd, R., and Davies, B. (1996). A telemanipulator system as an assistant and training tool for penetrating soft tissue. *Mechatronics*, **6**(4): 423–436.

Zivanovic, A. and Davies, B. (2000). A robotic system for blood sampling. *IEEE Transactions on Information Technology in Biomedicine*, **4**(1): 8–14.